1
2
3
Representational dynamics of task context and its influence on visual object processing

Hebart, M. N.[1], Bankson, B. B.[1], Harel, A.[2], Baker, C. I.[1]*, & Cichy, R. M.[3]*

[1]Section on Learning and Plasticity, Laboratory of Brain and Cognition, National Institute of Mental Health, National Institutes of Health, Bethesda, MD 20892, USA.

[2]Department of Psychology, Wright State University, Dayton, OH 45435, USA.

[3]Department of Education and Psychology, Free University of Berlin, 14195 Berlin, Germany.

* these authors contributed equally

Abbreviated title (50/50 characters): Time course of task and object category processing

Correspondence should be addressed to:

Martin N. Hebart
Laboratory of Brain and Cognition
National Institute of Mental Health
Building 10 Room 4C108
10 Center Drive
Bethesda, MD 20814
martin.hebart@nih.gov

Number of pages: 22
Number of figures: 5
Number of words: Abstract: 226, Significance Statement: 117, Introduction: 524, Discussion: 1552

Conflict of Interest: The authors declare no competing financial interests.

Abstract

Object recognition is commonly described as a feedforward process, yet the tasks we carry out often affect what information in visual stimuli is diagnostic and may influence their processing. Surprisingly little is known about how task context is processed and when and how it interacts with the emerging representation of objects. Here we used magnetoencephalography (MEG) and multivariate decoding to investigate the temporal dynamics of task and object processing and their interaction. Participants viewed objects while we varied task context on a trial-by-trial basis, using both high-level conceptual and low-level perceptual tasks. Time-resolved multivariate decoding and temporal cross-classification revealed multiple distinct yet overlapping stages of task processing from the onset of a trial, likely reflecting a sequence of visual, semantic, mnemonic, and rule-related task representations. Object decoding was stronger in conceptual than perceptual tasks, with differences emerging around 530 ms after object onset. However, object decoding generalized well between task contexts, indicating differently strong but qualitatively similar brain responses. Using model-based MEG-fMRI fusion, we found that frontoparietal areas were strongly dominated by information about task context throughout the trial, while occipitotemporal regions reflected a mixture of both task and object category indicating their parallel encoding in the same brain area. Together, our results reveal the temporal evolution of task context representations and suggest that the impact of task context during object processing occurs late in time.

Significance Statement

While much work in the vision sciences has focused on perceptual processing of visual stimuli, much less is known about the task context in which these stimuli occur. Here we studied the neural dynamics of task context and how it influences object processing. Using MEG, multivariate decoding and MEG-fMRI fusion, we reveal that task context evolves in multiple distinguishable yet overlapping processing stages, affecting object processing late in time. While frontoparietal regions were dominated by task, occipitotemporal regions exhibited a mixture of both task and object information. Our findings highlight the importance of temporal information in unravelling different stages of task processing and demonstrate the value of model-based MEG-fMRI fusion for a spatiotemporal analysis of cognitive processes.

Introduction

Our behavioral goals strongly influence how we interpret and categorize the objects around us. For example, the way in which we perceive and react towards a painting can vary quite dramatically when judging its period of art, whether it is hand-painted or a print, or whether it contains an animal or not. Despite the importance of task context in our everyday life, much work on the neural processing of objects has focused on single contexts only (e.g. fixation or discrimination). In part, this reflects the common view of object recognition as a hierarchical feedforward process localized to occipitotemporal cortex (Riesenhuber and Poggio, 2002; Serre et al., 2007; DiCarlo et al., 2012), with independent task-related processing in prefrontal and parietal cortex (Duncan, 2010). However, recent work suggests that task context can impact object representations not only in frontoparietal regions, but also in occipitotemporal visual cortex (Harel et al., 2014; Erez and Duncan, 2015; Bracci et al., 2017). In particular, task context has been reported to affect the strength (Erez and Duncan, 2015; Bracci et al., 2017) and qualitiative nature (Harel et al., 2014) of response patterns in occipitotemporal visual cortex.

While these studies demonstrate *where* in the brain task affects object processing, due to the low temporal resolution of fMRI they leave open the critical questions of (1) *when* the impact of task on object representations emerges and (2) *how* task is represented across time. Answers to these questions allow distinguishing alternative accounts for the mediating effects of task on object processing and in that way provide important insights into the neural mechanisms underlying task and object category. For example, changes in occipitotemporal cortex in response to task context could reflect an expectation-related top-down modulation of feedforward processing (Kok et al., 2012; Kok et al., 2013), potentially affecting the initial responses to visual stimuli. Alternatively, these responses may reflect a late, modulatory influence of task (McKee et al., 2014; see also Emadi and Esteky, 2014).

Here we studied the time course of the processing of task context and the effect of task on object category processing using magnetoencephalography (MEG) and time-resolved multivariate decoding (Carlson et al., 2013; Van de Nieuwenhuijzen et al., 2013; Cichy et al., 2014; Isik et al., 2014; Clarke et al., 2015; Kaiser et al., 2016). We measured the brain responses to object categories in four different task contexts, and used multivariate pattern classification to resolve the temporal dynamics of object category and task context, as well as their interaction. To locate the time-resolved task context and object category dynamics in the brain, we conducted model-based MEG-fMRI fusion (Cichy et al., 2014), using fMRI data from a previous study employing the same task (Harel et al., 2014). We found task context to be represented in a cascade of different processing stages across the time course of the trial. Task context affected the strength of object category representations late in time, however, we found no evidence for qualitatively different processing of objects between task types. MEG-fMRI fusion revealed strong task-related effects in frontoparietal regions, whereas task and category-related effects were mixed in occipitotemporal brain areas, suggesting their parallel processing of task and category.

Materials and Methods

Participants

124   22 healthy volunteers with normal or corrected-to-normal visual acuity took part in the study.
125   Five participants were excluded due to at least one of the following exclusion criteria: behavioral
126   performance below 90 % correct, excessive artifacts, or incomplete or corrupted recordings. Data
127   from the remaining 17 participants (8 female, mean age 25.12, SD = 5.16) were used in all
128   analyses throughout the study. All participants gave written informed consent as part of the study
129   protocol (93-M-0170, NCT00001360) prior to participation in the study. The study was approved
130   by the Institutional Review Board of the National Institutes of Health and was conducted
131   according to the Declaration of Helsinki.
132
133   *Experimental Design and Stimuli*
134
135   The goal of this study was to investigate how task context is represented across time and when
136   and how task context modulates the processing of visual object categories. For that purpose, we
137   chose four tasks that could be carried out on a set of object images, two targeting low-level
138   perceptual dimensions of the images, and two high-level conceptual dimensions (Figure 1A).
139   The perceptual dimensions were Color (red / blue) and Tilt (clockwise / counterclockwise), and
140   the conceptual dimensions were Content (manmade / natural) and Size (real world, large / small
141   relative to an oven). Object images were chosen from 8 different categories (Figure 1B):
142   Butterfly, cow, dresser, flower, motorbike, skate, tree, and vase. For each of the 8 object
143   categories, we chose five different image exemplars. To allow participants to perform the Color
144   and Tilt tasks, each object was presented with a thin red or blue outline, and objects were either
145   tilted 30 degrees clockwise or counterclockwise relative to the principal axis of the object. The
146   combination of stimulus types led to 160 unique stimulus combinations (8 categories × 5
147   exemplars × 2 colors × 2 tilts). Each stimulus was presented once in each task context, making a
148   total of 640 stimulus presentations per participant. The presentation order of these stimulus-task
149   combinations was randomized. In addition, we interspersed 80 catch trials that were chosen to be
150   random combinations of task and stimulus (see below).
151   All stimuli were presented on black background with a white central fixation cross
152   present throughout the experiment. Object images were greyscale cropped images of objects and
153   were a subset selected from a previous fMRI study (Harel et al., 2014). Both task cues (e.g.
154   'Content') and possible responses (e.g. 'manmade' or 'natural') were shown as words in white
155   font. Task cues were always presented centrally and possible responses were shown left and right
156   of fixation.
157
158   *Procedure*
159
160   Prior to the experiment, participants were familiarized with the task by carrying out 36 randomly
161   chosen trials outside of the MEG. For the actual experiment, participants were seated in an
162   electromagnetically shielded MEG chamber with their head placed in the mold of the dewar
163   while stimuli were backprojected on a translucent screen in front of them (viewing distance: 70
164   cm, image size: 6 degrees of visual angle). Each trial was preceded by a white fixation cross (0.5
165   s) that turned green (0.5 s) to prepare participants for the upcoming trial. A trial consisted of
166   three major components: (1) A task cue which indicated the relevant task for the trial, (2) an
167   object stimulus which was categorized according to the task, and (3) a response-mapping screen
168   which indicated the task-relevant response options left and right of fixation (Figure 1C). Based
169   on these components, in the following we separate each trial into three different time periods: a

170 "Task Cue Period", an "Object Stimulus Period", and a "Response Mapping Period". Each trial
171 lasted 5 s. A trial began with the Task Cue Period consisting of the presentation of a task cue (0.5
172 s) followed by a fixation cross (1.5 s). This was followed by the Object Stimulus Period
173 consisting of the presentation of an object stimulus (0.5 s) followed by another fixation cross (1.0
174 s). Finally, the trial ended with the Response Mapping Period during which a response-mapping
175 screen was displayed (1.5 s). Participants responded with the left or right index finger using an
176 MEG-compatible response box. In addition to the button press, participants were instructed to
177 make an eye blink during the response period to minimize the contribution of eye blink artifacts
178 to other time periods. The order of the options on the response-mapping screen was intermixed
179 randomly to prevent the planning of motor responses before the onset of the response screen
180 (Hebart et al., 2012).
181   Participants were instructed to encode the task rule as soon as being presented with the
182 task cue and to apply it immediately to the stimulus. To encourage this strategy, they were asked
183 to respond as fast and accurately as possible. To enforce a faster application of task to object
184 category, we introduced catch trials for which the fixation period between stimulus offset and
185 response-mapping screen onset was shortened from 1.0 s to 0.2 s. The experiment consisted of
186 20 runs of 36 trials each (32 experimental trials, 4 catch trials).
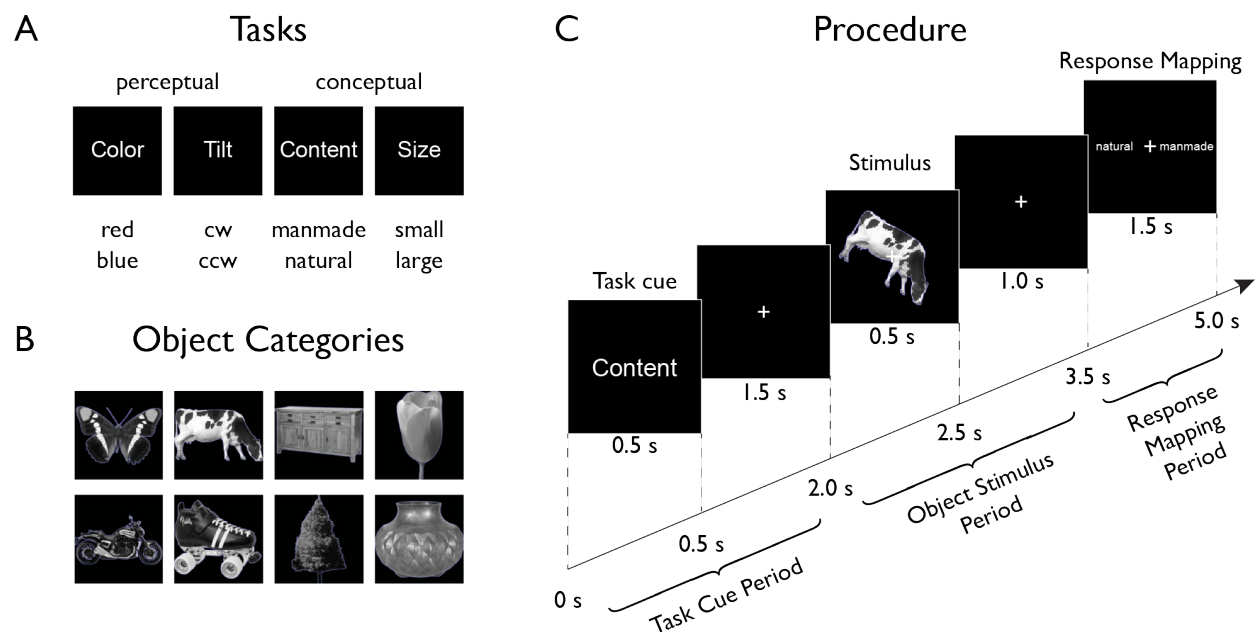187

188
189 **Figure 1**. Experimental paradigm. On each trial (Procedure depicted in Panel **C**), participants were presented with a
190 stimulus from one of eight different object categories (Panel **B**) embedded in one of four task contexts (Panel **A**, top)
191 indicated at the beginning of each trial. Participants carried out a task that either targeted low-level features
192 (perceptual tasks) of the object or its high-level, semantic content (conceptual tasks). After a short delay, a response-
193 mapping screen was shown that presented the possible response alternatives (Panel **A**, bottom) in random order
194 either left or right of fixation to decouple motor responses from the correct response.
195

MEG Recordings and Preprocessing

197
198 MEG data were collected on a 275 channel CTF system (MEG International Services, Ltd.,
199 Coquitlam, BC, Canada) with a sampling rate of 1,200 Hz. Recordings were available from 272
200 channels (dead channels: MLF25, MRF43, MRO13). Preprocessing and data analysis were

4

201 carried out using Brainstorm (version 02/2016, Tadel et al., 2011) and MATLAB (version
202 2015b, The Mathworks, Natick, MA). The specifics of preprocessing and multivariate decoding
203 (see below) were based on previously published MEG decoding work (Cichy et al., 2014;
204 Grootswagers et al., 2016) and fine-tuned on a pilot subject that did not enter the final data set.
205 MEG triggers were aligned to the exact presentation time on the screen that had been recorded
206 using an optical sensor attached to the projection mirror. Data were epoched in 5.1 s trials,
207 starting 100 ms prior to the onset of the task cue and ending with the offset of the response-
208 mapping screen. Then, data were bandpass filtered between 0.1 and 300 Hz and bandstop filtered
209 at 60 Hz including harmonics to remove line noise.
210   To further increase SNR and to reduce computational costs, we carried out (1) PCA
211 dimensionality reduction, (2) temporal smoothing on PCA components, and (3) downsampling
212 of the data. For PCA, data were concatenated within each channel across all trials. After PCA,
213 the components with the lowest 1 % of the variance were removed (maximum removal: 50 % of
214 components). All further analyses were conducted on the reduced set of principal components.
215 Then, data were normalized relative to the baseline period (for task decoding: -0.1 to 0 s, for
216 object category decoding: 1.9 to 2.0 s). To this end, for each channel we calculated the mean and
217 standard deviation of the baseline period and subtracted this mean from the rest of the data
218 before dividing it by the standard deviation (univariate noise normalization). Finally, the
219 components were temporally smoothed with a Gaussian kernel of $\pm$ 15 ms half duration at half
220 maximum, and downsampled to 120 Hz (621 samples / trial).
221
222 *Time-resolved Multivariate Decoding*
223
224 Multivariate decoding was carried out using custom-written code in MATLAB (Mathworks,
225 Natick, MA), as well as functions from The Decoding Toolbox (Hebart et al., 2015), and
226 LIBSVM (Chang and Lin, 2011) using linear support vector machine classification (C = 1).
227 Classification was conducted for each participant separately in a time-resolved manner, i.e.
228 independently for each time point. Each pattern that entered the classification procedure
229 consisted of the principal component scores at a given time point. In the following we describe
230 one iteration of the multivariate classification procedure that was carried out for the example of
231 object category classification. In the first step, we created supertrials by averaging 10 trials of the
232 same object category without replacement (Isik et al., 2014). In the next step, we separated these
233 supertrials into training and testing data, with one supertrial pattern per object category serving
234 as test data and all other supertrial patterns as training data. This was followed by one-vs-one
235 classification of all 28 pairwise comparisons of the 8 object categories (chance-level 50 %). To
236 test the trained classifier on the left-out data, we compared the two predicted decision values and
237 assigned an accuracy of 100 % if the order of the two test samples was predicted correctly and an
238 accuracy of 0 % if the order was the opposite (for two samples and two classes this is
239 mathematically equivalent to the common area-under-the-curve measure of classification
240 performance and represents a classification metric that is independent of the bias term of the
241 classifier). In a last step, the resulting pairwise comparisons were averaged, leading to an
242 estimate of the mean accuracy across all comparisons. This training and testing process was then
243 repeated for each time point. This completes the description of one multivariate classification
244 iteration for the decoding of object category. The procedure for task classification was
245 analogous, with 4 tasks and 6 pairwise combinations. To achieve a more fine-grained and robust
246 estimate of decoding accuracy, we ran a total of 500 such iterations of trial averaging and

247   classification, and the final accuracy time series reflects the average across these iterations. This
248   provided us with time-resolved estimates of MEG decoding accuracy for object category and
249   task classification, respectively.
250
251   *Temporal Generalization of Task*
252
253   To investigate whether the nature of task-related information remained stable across time or
254   whether it changed, we carried out cross-classification across time, also known as the temporal
255   generalization method (King and Dehaene, 2014). The rationale of this method is that if a
256   classifier can generalize from one time point to another, this demonstrates that the
257   representational format is similar for these two time points. If, however, a classifier does not
258   generalize, then under the assumption of stable noise this indicates that the representational
259   format is different. To carry out this analysis, we repeated the same approach as described in the
260   previous section, but instead of testing a classifier only at a given time point, we tested the same
261   classifier for all other time points separately. This cross-classification analysis was repeated with
262   each time point once serving as training data, yielding a time–time decoding matrix that captures
263   classifier generalization performance across time.
264
265   *Model-based MEG-fMRI Fusion for Spatiotemporally-Resolved Information*
266
267   To resolve task and category-related information both in time and space simultaneously, we
268   carried out RSA-based MEG-fMRI fusion (Cichy et al., 2014, 2016). RSA allows comparison of
269   brain patterns across modalities in terms of pattern dissimilarity, abstracting from the activity
270   patterns of measurement channels (e.g. MEG sensors) to all pairwise distances of those patterns
271   in form of a representational dissimilarity matrices (RDMs). RSA-based MEG-fMRI fusion
272   allows a researcher to ask the following question: At what point in time does the representational
273   structure in a given brain area (as determined from fMRI) match the representational structure
274   determined from the time-resolved MEG signal? The reasoning for this approach is that if the
275   fMRI RDM of a brain region and the MEG RDM of a time point show a correspondence, this
276   suggests that there is a shared representational format in a given brain location and at a given
277   point in time. Here we apply this approach to investigate the spatiotemporal evolution of object
278   category and task representations.
279   FMRI RDMs for each combination of task and category ($4 \times 8 = 32 \times 32$ matrices) were
280   available from five regions of interest (ROIs) in 25 participants who took part in a separate study
281   employing the same task (Harel et al., 2014). None of these participants overlapped with the
282   sample from the MEG study. The major difference between the MEG and the fMRI experiments
283   were (1) that the fMRI study used an extended set of 6 tasks and (2) the exact timing of each trial
284   was slower and jittered in the fMRI study. Details about data preprocessing have been described
285   previously (Harel et al., 2014). RDMs were based on parameter estimates in a GLM for each
286   condition which were converted to *t*-values (univariate noise normalization). Each entry in the
287   matrix reflects 1 minus the correlation coefficient of the *t*-values across conditions, calculated
288   separately for each ROI. RDMs were reduced to the relevant four task types. The five ROIs were
289   early visual cortex (EVC), object-selective LO and pFS, lateral prefrontal cortex (lPFC) and
290   posterior parietal cortex (PPC). EVC, LO and pFS were defined based on contrasts in an
291   independent visual and object localizer session, and lPFC and PPC were defined by a

6

292 combination of anatomical criteria and responses in the functional localizer session to the
293 presence of objects.
294   For better comparability to this previous study, we created correlation-based MEG
295 pattern dissimilarity matrices for all combinations of task and object category. In particular, for
296 each combination of task and category, we created a mean pattern, yielding a total 32 brain
297 patterns per participant (8 categories × 4 tasks). We then ran a Pearson correlation between all
298 patterns and converted these similarity estimates to dissimilarity estimates (using 1 minus
299 correlation), providing us with a 32 × 32 RDM for each time point and participant.
300   Since different groups of participants were tested in the fMRI and MEG studies, we used
301 the group average pattern dissimilarity matrices of each modality as the best estimate of the true
302 pattern dissimilarity. These RDMs were symmetrical around the diagonal, so we extracted the
303 lower triangular component of each pattern dissimilarity matrix and converted them to vector
304 format for further analyses, in the following referred to as representational dissimilarity vector
305 (RDV).
306   For a given brain region, we conducted MEG-fMRI fusion by calculating the squared
307 Spearman correlation between the fMRI RDV and the MEG RDV for each time point separately.
308 The squared correlation coefficient is mathematically equivalent to the coefficient of
309 determination (R^2) of the fMRI RDV explaining the MEG RDV. This approach was repeated for
310 each fMRI RDV of the five ROIs, providing us with five time courses of representational
311 similarity between MEG and fMRI.
312   While MEG-fMRI fusion provides a temporal profile of representational similarities for a
313 given brain region, these MEG-fMRI fusion time courses do not distinguish whether MEG-fMRI
314 representational similarities reflect task, object category, or a mixture of the two. To disentangle
315 task and object category-related information with MEG-fMRI fusion, we extended this approach
316 by introducing model RDMs of the same size (32 × 32). These RDMs reflected the expected
317 dissimilarity for the representation of task and category, respectively, with entries of 1 for high
318 expected dissimilarity (different task / category) and 0 for low expected dissimilarity (same task /
319 category). This model-based MEG-fMRI fusion approach was carried out using commonality
320 analysis (Seibold and McPhee, 1979), a variance decomposition approach that allows estimating
321 the shared variance between more than two variables (see Greene et al., 2016, for a similar
322 approach using multiple model RDMs). For a given brain region and time point, these variables
323 reflect (1) an MEG RDV, (2) an fMRI RDV and (3) the two model RDVs for task and object
324 category representations.
325   A schematic of this model-based MEG-fMRI fusion is shown in Figure 5A. We
326 conducted commonality analysis by comparing two squared semi-partial correlation coefficients
327 (Spearman correlation), one reflecting the proportion of variance shared between MEG and
328 fMRI partialling out all model variables excluding the variable of interest (e.g. task) from fMRI,
329 and the other reflecting the proportion of shared variance when partialling out all model variables
330 from fMRI including this variable of interest. The difference between both coefficients of
331 determination (R^2) then provides the commonality, which is the variance shared between MEG
332 and fMRI that is uniquely explained by the variable of interest. Formally, the commonality at
333 time t and location j can be described as:
334
335 $$C_{X_t,(Y_j,A)} = R^2{}_{X_t,(Y_j.B)} - R^2{}_{X_t,(Y_j.A,B)}$$
336

337   where *X* reflects MEG, *Y* reflect fMRI, *A* reflects task, and *B* reflects object category. Note that
338   this variable can become slightly larger than the total R^2 or slightly negative, due to numerical
339   inaccuracies or the presence of small suppression effects (Pedhazur, 1997). In addition,
340   commonality coefficients always reflect the shared variance relative to a target variable (in our
341   case MEG), but depending on the relationship between the variables the estimate of shared
342   variance can change when a different target variable is used (in our case fMRI). In the present
343   study, the pattern of results was comparable irrespective of which variable served as a target
344   variable.
345
346   *Statistical Testing*
347
348   Throughout this article, we used a non-parametric, cluster-based statistical approach to
349   test for time periods during which the group of participants showed a significant effect (Nichols
350   and Holmes, 2002), and bootstrap sampling to determine confidence intervals for peak latencies
351   and peak latency differences. We did not compute statistics in time periods after the onset of the
352   response-mapping screen, because (1) these time periods were corrupted by the instructed eye
353   blinks and (2) information about task is contained in the response-mapping screen, making it
354   difficult to uniquely assign these responses to task or response-mapping screen. For object
355   category-related responses we did not compute statistics for time periods prior to the onset of the
356   object stimulus, because it was not reasonable to assume that these periods would contain
357   information about the category before its identity is revealed. For completeness, however, we
358   plot these results in Figures 2 and 3. Please note that the pattern of results reported is very similar
359   when including these time periods into our statistical analyses.
360
361   <u>Non-parametric Cluster-based Statistical Approach</u>
362   The cluster-based approach consists of two steps: first defining clusters as neighboring
363   time points that all exceed a statistical cutoff (cluster-inducing threshold), and second
364   determining significant cluster size.
365   For the first step – the definition of a cluster-inducing threshold – we ran a sign-
366   permutation test. The null hypothesis is that any directional effect in the given sample of
367   participants simply came about by chance. To test whether our sample was part of this null
368   distribution, for each time series of accuracies we created all possible sign-permutations of
369   measured accuracy values (2^{17} = 131,072), and for each of these permutations generated a *t*-value
370   for each time point. The permutations provided a null distribution of *t*-values of the group effect
371   for each time point. The cluster-inducing threshold was defined as the 95th percentile of the
372   distribution at each time point (equivalent to *p* < 0.05, one-sided).
373   For the second step – determining significant clusters – we determined the maximum
374   cluster size in each permutation (Nichols and Holmes, 2002). Using this null distribution, we
375   determined whether candidate clusters in the original time series exceeded the 95th percentile of
376   maximum cluster sizes (equivalent to *p* < 0.05, one-sided). This provided us with significant
377   clusters at the pre-specified statistical cutoffs.
378   For temporal generalization matrices, we extended the cluster-based approach described
379   above to two dimensions, revealing significant 2D clusters. Because of computational
380   limitations, we ran only a subset of 10,000 permutations drawn randomly without replacement
381   from all available permutations.

8

382   For model-based MEG-fMRI fusion, we used the two-step approach as described above.
383   However, instead of running a sign-permutation test across participants, we conducted a
384   randomization test for which we created 5,000 MEG similarity matrices for each of the five
385   ROIs. These matrices were based on random permutations of the rows and columns of the group
386   average MEG similarity matrix (Kriegeskorte et al., 2008). We then carried out model-based
387   MEG-fMRI fusion using these matrices to create an estimated null distribution of information
388   time courses for each ROI. For each time point in each ROI, a cluster-inducing threshold was
389   determined by choosing the 95th percentile of this estimated null distribution (equivalent to $p <$
390   0.05, one-sided). This was followed by determining the maximum cluster sizes across all
391   permutations as described above, but across all ROIs to correct for multiple comparisons
392   (equivalent to $p < 0.05$, one-sided, corrected for multiple comparisons across ROIs).
393
394   <u>Determining Confidence Intervals for Peak Latencies</u>
395   We used bootstrap sampling to estimate the 95 % confidence intervals (CI) of peak
396   latencies and peak latency differences, respectively. For each iteration of the bootstrap sampling
397   approach, we calculated a time course based on the bootstrap sample. For multivariate decoding
398   analyses, this was a time course of accuracy from an average of n=17 time courses of decoding
399   accuracy sampled with replacement from the pool of subjects. For MEG-fMRI fusion, this was a
400   time course of commonality coefficients, generated by sampling n=17 time courses of MEG
401   similarity matrices from the pool of subjects with replacement, averaging them, and repeating the
402   model-based MEG-fMRI fusion approach as described above. For each bootstrap sample time
403   course, we then calculated timing estimates in the relevant time periods (for peak latency: timing
404   of maximum, for peak latency difference: time difference between maxima). This process was
405   repeated (100,000 times for multivariate decoding and 5,000 times for MEG-fMRI fusion),
406   which generated a distribution of timing estimates. The 2.5 and 97.5 percentiles of this
407   distribution reflect the 95 % confidence interval of the true timing estimate. Since we
408   downsampled our data (bin width: 8.33 ms), the confidence intervals were conservative and
409   overestimated by up to 16.67 ms.
410
411   **Results**
412
413   *Behavioral Results*
414
415   Participants provided correct responses on average on 97.19 % of trials (*SD*: 2.40) and had a
416   mean response time of 712.2 ms (*SD*: 121.8), with no significant differences between tasks
417   (accuracy: $F(3,48) = 0.6938$, RT: $F(3,48) = 0.039$) or between object categories (accuracy:
418   $F(7,112) = 0.6024$, RT: $F(7,112) = 0.5431$). On average, participants missed responses or
419   responded too slowly (RT > 1,600 ms) in only 1.80 % of all trials (*SD*: 2.26). We included all
420   trials in further analyses because (1) imbalances in the number of trials per condition would
421   complicate multivariate analyses, requiring subsampling which would make the results less
422   sensitive, and (2) there were no differences in accuracy or RT across tasks or objects, making it
423   unlikely that the results would be biased by including a very small fraction of missed or incorrect
424   trials.
425
426   *Time-resolved Representation of Task Context and Object Category*
427

428   The primary aim of this study was to characterize the temporal evolution of task context
429   representations in the human brain and elucidating at what time task context affects object
430   category processing. We thus separately analyzed task and object category-related brain signals
431   using time-resolved multivariate decoding across the trial (see Figure 1C). This allowed us to
432   describe and compare the temporal profiles of the two resulting classification time courses, one
433   for object category averaged across task, and one for task averaged across object category.

434   In the following, we describe and report results from the "Task Cue Period" (0 to 2,000
435   ms) from onset of the task cue to onset of the object stimulus, and the "Object Stimulus Period"
436   (2,000 to 3,500 ms) from onset of the object stimulus to onset of the response screen. We did not
437   statistically analyze the ensuing "Response-Mapping Period" (3,500 ms to 5,000 ms), because it
438   was contaminated by instructed blinks and response screen-related processes (see *Materials and*
439   *Methods, Statistical Testing)*. For completeness, we visualize results from this Response-
440   Mapping Period in Figures 2 and 3.

441   *Task Cue Period.* Task-related information rose rapidly in response to the task cue,
442   peaking around 100 ms (peak of group mean: 100 ms, 95 % CI: 96-121 ms). This was followed
443   by a slow decay of information that remained significantly above chance until ~1,200 ms after
444   cue presentation, outlasting the offset of the word cue by ~700 ms. Around 1,800 ms (~200 ms
445   prior to onset of the object stimulus) task information was again found to be significantly above
446   chance. As expected, during this time period – prior to the presentation of the object stimulus –
447   classification of object category was at chance.

448   *Object Stimulus Period.* After onset of the object stimulus at 2,000 ms, object category
449   information increased sharply, peaking around 100 ms later (peak of group mean: 2,104 ms, 95
450   % CI: 100-108 ms). This was followed by a gradual decline that remained significantly above
451   chance until the onset of the response-mapping screen at 3,500 ms. This rapid increase in
452   category-related information was accompanied by a slow rise of task-related information peaking
453   around 600 ms after object onset (peak of group mean: 2,638 ms, 95 % CI: 2,517-2,825 ms).
454   Information about task then remained well above-chance until the presentation of the response-
455   mapping screen.

456   Together, these results show that both the presentation of task cue and object stimulus
457   lead to rapid cortical processing. In addition, they suggest that maintained or reactivated task-
458   related information that is present before object onset becomes gradually and increasingly
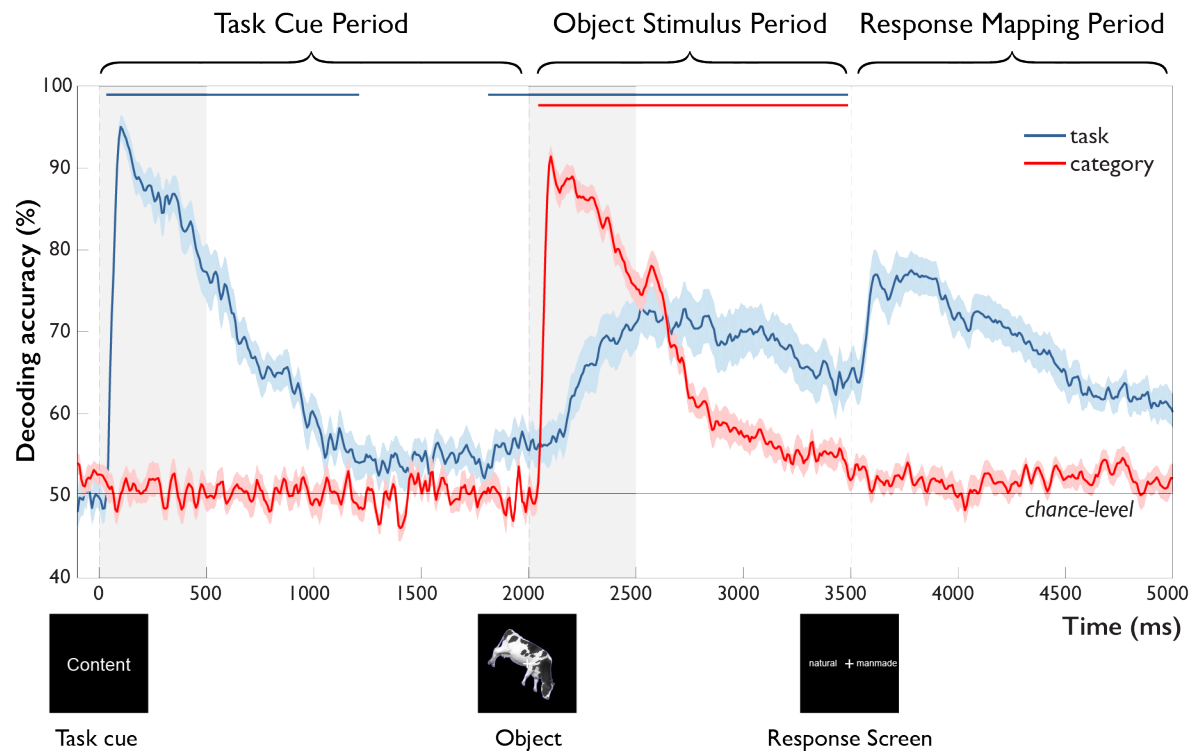459   relevant during object category processing.
460

Figure 2. Time-resolved multivariate decoding of task and object category across the trial. After onset of the task cue (Task Cue Period), task-related accuracy increased rapidly, followed by a decay back towards chance, and was significantly above-chance ~200 ms prior to object onset. In contrast, category-related accuracy was at chance as expected. After onset of the object stimulus (Object Stimulus Period), object category-related accuracy increased rapidly, decaying back to chance with the onset of the response-mapping screen. This was paralleled by a gradual increase in task-related accuracy, peaking ~600 ms after object onset and remaining high until onset of the response-mapping screen. Error bars reflect SEM across participants for each time-point separately. Significance is indicated by colored lines above accuracy plots (non-parametric cluster-correction at $p < 0.05$). Time periods after the onset of the response-mapping screen were excluded from statistical analyses, because they were contaminated by instructed eye-blinks and responses to the response-mapping screen itself, but are shown for completeness (see Methods and Results).

Multiple Stages of Task Processing Revealed by Temporal Generalization Analysis

The decoding of task at different time points as described above characterizes the temporal progression of task-related information across the trial. However, these results alone do not allow distinguishing whether the decoding of task reflects a single or a sequence of multiple cognitive processes across time. There are three pertinent candidates that might explain task decoding at different time periods. For one, early decoding of task after task cue onset may reflect an early visual representation of the task cue that is maintained in short-term memory and accessed when the object stimulus appears in order to carry out the task. Alternatively, the task representation during object processing may reflect an abstract representation of the participant's choice that has been formed after initial visual and semantic processing of the task cue. Finally, the visual information about the task cue may reflect a more abstract representation of task rule that is maintained and applied to the object stimulus representation.

To characterize the processing stages of task, we conducted a temporal generalization analysis using multivariate cross-decoding that reveals the temporal evolution of representational

11

490   formats of task (Meyers et al., 2008; King and Dehaene, 2014). To this end, we trained a
491   classifier at each time point during the trial to distinguish the four different tasks and then tested
492   it at all other time points, providing us with a time × time temporal generalization matrix. The
493   shape of the results informs about similarities and differences in the way information is
494   represented across time. If the results show classification that generalizes to all time points, i.e. if
495   the entire matrix carries information, this indicates that task information is maintained in a
496   similar format across the entire trial. If the results show very little generalization across time, i.e.
497   above-chance accuracies only very close to the diagonal, this indicates that task representation is
498   highly dynamic across the trial. And if there are several quadratic blocks of cross-classification
499   around the diagonal, this indicates that task representations change abruptly in different periods
500   of the trial.

501   The temporal cross-classification analysis revealed multiple separate, but partially
502   overlapping stages of processing after the onset of the task cue (Figure 3A). At a coarse level, the
503   temporal generalization matrix exhibited a block structure within the Task Cue Period and
504   Object Stimulus Period (*Within-Period Cross-Decoding*, Figure 3B, left panel). This indicates a
505   shared representational format *within* each time period of the trial, but a largely different
506   representational format *between* those time periods, and an abrupt change in the representational
507   format of task after onset of the object stimulus. Since visual and semantic representations of the
508   task cue are likely to emerge early in the Task Cue Period, this result speaks against a visual or
509   semantic representation during the Object Stimulus Period. However, this separation was not
510   complete: some time points exhibited cross-decoding between time periods (*Between-Period
511   Cross-Decoding*, Figure 3B, middle and right panel), as evidenced by the off-diagonals of the
512   generalization matrix (i.e. training time 0 to 2,000 ms, testing time 2,000 to 3,500 ms, and vice
513   versa). This indicates a partially shared representational format between these periods of the trial.

514   Next we focused on the fine-grained dynamics of task processing in the Task and Object
515   Cue Period, respectively. During the Task Cue Period (0 to 2,000 ms) the results revealed a
516   block of increased cross-classification lasting from ~100 to ~600 ms after cue onset. This block
517   likely reflects the time the task cue was available to visual cortex (accounting for the delay
518   between stimulus onset and cortical processing). After offset of the task cue at 500 ms and prior
519   to the onset of the object stimulus at 2,000 ms, information continued to be present and was
520   found to generalize to other time points in the Task Cue Period. This reinforces the notion that
521   information about task was actively maintained throughout the Task Cue Period, as suggested by
522   the time-resolved decoding analysis presented above. This short-term memory representation of
523   task exhibited temporal generalization to most time points of the Task Cue Period, including the
524   visual presentation of the task cue, indicating that the short-term representation of task included
525   visual and semantic properties of the task cue. During the Object Stimulus Period, there was a
526   gradual build-up of task-related information until ~200 ms after object onset. At that point, the
527   results exhibited high levels of cross-classification until the onset of the response-mapping
528   screen, indicating a maintained representation of task context that did not change until the onset
529   of the response mapping screen.

530   Significant cross-classification between the Task Cue and Object Stimulus Period was
531   evident in two distinct phases. First, there was generalization from the Task Cue Period to the
532   first ~200 ms of the Object Stimulus Period (training time ~300 to 2,000 ms, testing time 2,000
533   to ~2,200 ms, Figure 3B, middle panel), possibly reflecting a maintained short-term
534   representation that continued until the task rule could be applied to the object. Second, there was
535   generalization from the end of the Task Cue Period to the Object Stimulus Period (training time

536 ~1,500 to 2,000 ms, testing time 2,000 ms to ~3,300 ms, Figure 3B, right panel), indicating that
537 the short-term memory representation of task was similar to the representation during application
538 of the task rule to the object. Interestingly, this cross-classification was specific to the late short-
539 term memory representation and did not generalize to other time points of the Task Cue Period.
540 Note that this cannot be explained by a representation of the correct response, because
541 participants could not know the correct response during this short-term memory representation
542 prior to the presentation of the object. Together, this pattern of results suggests that the
543 representation of task during the Object Stimulus Period likely does not reflect visual or semantic
544 processing of the task cue (which would predict cross-classification from the early Task Cue
545 Period); nor does it reflect only a representation of the correct response. Rather, the results
546 indicate that participants form an abstract representation of task rule during the short-term
547 retention period prior to object onset, which they apply to the object stimulus when it is
548 presented.
549   In summary, the results indicate separate, but overlapping stages of task context
550 processing. These stages likely reflect a cascade of visual, semantic, and mnemonic processes
551 including an abstract representation of task rule which during object processing is converted into
552 an abstract behavioral choice reflected in the participant's response.

554 **Figure 3**. Results of temporal generalization
555 analysis of task. **A.** Temporal cross-classification
556 matrix. The y-axis reflects the classifier training
557 time relative to task cue onset, the x-axis the
558 classifier generalization time, and the color codes
559 the cross-classification accuracy for each
560 combination of training and generalization time.
561 The outline reflects significant clusters ($p < 0.05$,
562 cluster-corrected sign permutation test). Results
563 after the onset of the response-mapping screen are
564 not included in the statistical evaluation but are
565 shown for completeness. (see Results) **B.** Panels
566 that schematically indicate three patters in the
567 temporal generalization results. First, there was a
568 block structure (*Within-Period Cross-Decoding*)
569 separately spanning the Task Cue Period and the
570 Object Stimulus Period, indicating largely different
571 representations during the different periods of the
572 task (left panel). At the same time, there were two
573 separate patterns of temporal generalization in the
574 off-diagonals (*Between-Period I and Between-*
575 *Period II Cross-Decoding* illustrated in middle and
576 right panel, respectively*)*, indicating a shared
577 representational format between these time periods.
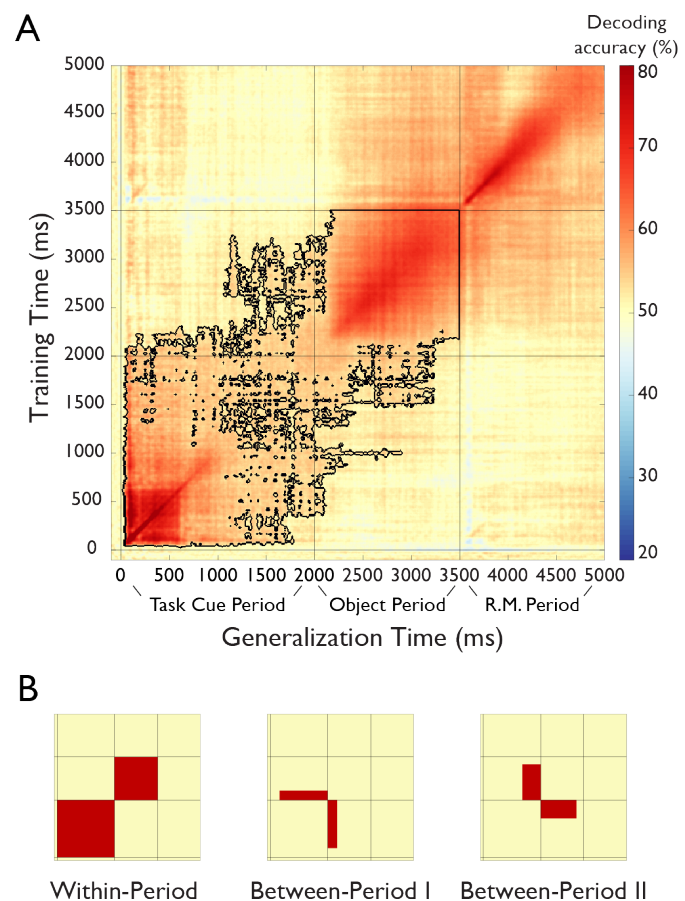
584 *Effects of Task Context on Object Category Representations*

586 The robust decoding of task context that increases during object processing raises the question
587 whether the task context representation is independent of object processing, or whether task
588 context influences object category representations. If object category processing is influenced by
589 task type, one prediction is that object information time courses would be different for different
590 task types. To investigate this question, we conducted time-resolved multivariate decoding of
591 objects separately for perceptual and conceptual task types and compared the time courses. The
592 results of this analysis are presented in Figure 4A. The overall time course of object decoding
593 was very similar for conceptual and perceptual tasks as compared to that reported for object
594 decoding across tasks, as expected (see *Time-resolved Representation of Task Context and*
595 *Object Category* and Figure 2): accuracies increased sharply after stimulus onset, followed by a
596 gradual decline, dropping back to chance level towards the end of the Object Period. Comparing
597 the decoding curves for conceptual and perceptual tasks directly revealed higher accuracies for
598 conceptual tasks. This result reveals that task context affects object representations late in time.
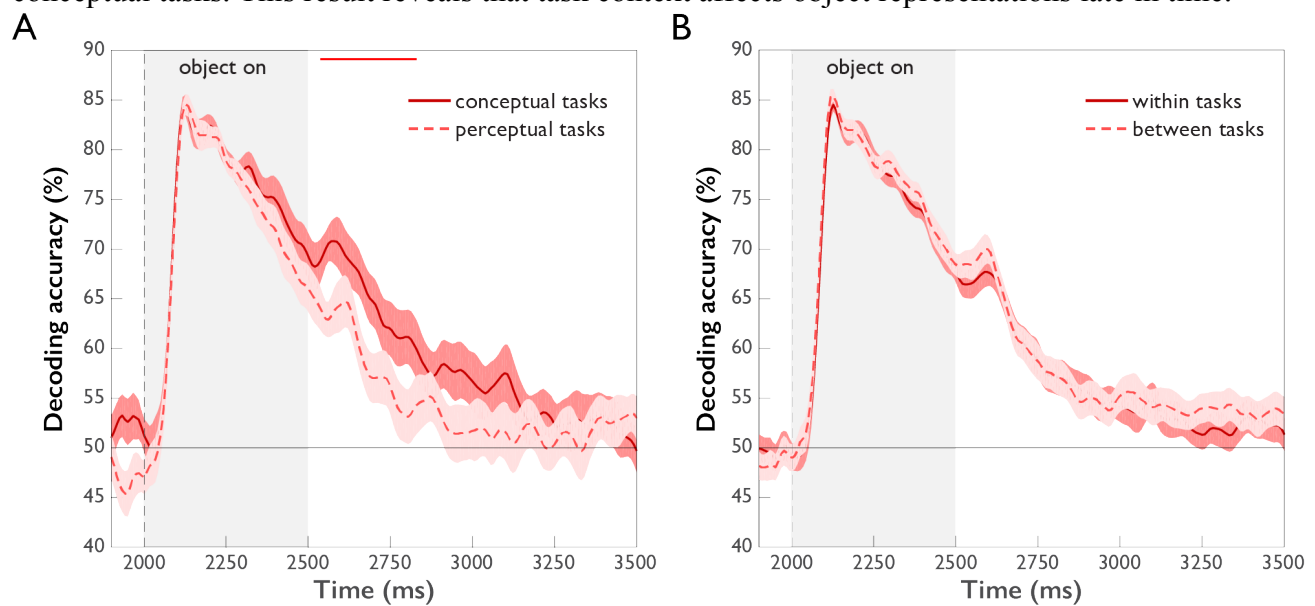

599
600
601 **Figure 4**. Comparison of object category decoding for different task types ($p < 0.05$, cluster-corrected sign
602 permutation test). Error bars reflect standard error of the difference of the means. **A.** Object category decoding
603 separated by perceptual and conceptual task types. Initially, category decoding for conceptual and perceptual tasks is
604 the same, followed by decoding temporarily remaining at a higher level for conceptual tasks than perceptual tasks
605 between 500 and 750 ms post stimulus onset. **B.** Object category decoding within and across task types. A classifier
606 was trained on data of different categories from one task type and tested either on category data from the same task
607 type (within tasks) or on category data from the other task type (between tasks). There was no difference in within
608 and between-task decoding.

609
610   In addition to these quantitative differences in object category representations across task
611 types, we investigated whether the object representations were qualitatively similar but
612 differently strong (more separable patterns), or whether they were qualitatively different across
613 task types (different patterns). To this end, we compared object category classification *within*
614 task to object category classification *between* tasks. The rationale of this approach is that if the
615 between task cross-classification accuracy is lower than the within task accuracy, this
616 demonstrates that the classifier cannot rely on the same source of information in these two
617 conditions, i.e. the patterns must be qualitatively different between tasks. The results of this
618 analysis are shown in Figure 4B. We did not find any differences in object decoding accuracies

14

619 within vs. between task types, indicating that the object category-related patterns were
620 qualitatively similar across time.
621   Together, our results reveal that task context affects object representations late in time
622 and provide further evidence for the notion that task affects the strength of object category
623 representations.
624
625 *Model-based MEG-fMRI Fusion for Spatiotemporally-Resolved Neural Dynamics of Task and*
626 *Object Category*
627
628 To investigate the cortical origin of the task and object category-related effects, we carried out
629 MEG-fMRI fusion based on representational similarity analysis (Cichy et al., 2014, 2016). We
630 calculated time-resolved MEG representational dissimilarity matrices (RDMs) for all
631 combinations of task and category and compared them to fMRI RDMs derived from brain
632 activity patterns from five ROIs of a previously-published study employing the same task (Harel
633 et al., 2014). Similarity between an fMRI ROI RDM and MEG RDMs indicates a
634 representational format common to that location and those time points. To separately assess the
635 contributions of object category and task to the representational similarity between MEG and
636 fMRI, we decomposed the shared variance between MEG and fMRI RDMs using commonality
637 analysis (Seibold and McPhee, 1979). This procedure identifies the portion of variance shared
638 between MEG and fMRI that is unique to either task of category (Figure 5A). The task and
639 category model RDMs were constructed based on the expected dissimilarity matrix for task
640 irrespective of category, and for category irrespective of task, respectively.
641   The results of this model-based MEG-fMRI fusion are shown in Figure 5B-F separately
642 for each ROI. The grey shaded area indicates the amount of variance captured by MEG-fMRI
643 fusion. Blue and red lines indicate the amount of variance in the MEG-fMRI fusion uniquely
644 explained by the task and object category model respectively.
645   In all ROIs and at most time points either the task or object category models explained
646 the majority of the shared variance between MEG and fMRI, as indicated by the close proximity
647 of the colored lines to the upper boundary of the grey shaded area. This result demonstrates that
648 task and category model RDMs are good models for describing the observed spatio-temporal
649 neural dynamics.
650   All regions carried information about task context and object category at some point
651 throughout the trial, indicating overlapping representations of task and object category
652 distributed across cortical location and time. However, regions differed in the predominance and
653 mixture of the represented content. Both PPC and lPFC were clearly dominated by effects of task
654 context, with much weaker object category-related commonality coefficients present in these
655 areas. These regions exhibited high task-related commonality coefficients both during the Task
656 Cue Period and the Object Stimulus Period. Interestingly, PPC exhibited significant task-related
657 commonality coefficients throughout the short-term retention period that were not found in lPFC,
658 which may speak towards a different functional role of these regions in the retention of task
659 rules.
660   In contrast to frontoparietal regions, occipitotemporal regions EVC, LO and pFS
661 generally exhibited weaker but significant task-related commonality coefficients than PPC and
662 lPFC. All three regions displayed significant task-related commonality coefficients in the Task
663 Cue Period. Interestingly, in the Object Stimulus Period all three regions exhibited a mixture of
664 task and object-category related commonality coefficients, indicating the concurrent encoding of

665   task and object category in these brain areas. Moreover, the relative size of task-related
666   commonalities increased gradually from EVC through LO to pFS, indicating an increasing
667   importance of task encoding when progressing up the visual hierarchy. In all five regions, after
668   onset of the object stimulus category-related commonality coefficients peaked earlier than task-
669   related commonality coefficients (all $p < 0.05$, based on bootstrap CI for differences in peaks),
670   mirroring the results of the time-resolved multivariate decoding analysis.

671   Together, we found that the spatiotemporal neural dynamics as revealed by model-based
672   MEG-fMRI fusion predominantly reflected task or object processing, with systematic differences
673   across cortical regions: While PPC and lPFC were dominated by task and PPC carried task
674   information throughout the Task Cue Period, EVC, LO and pFS exhibited a mixture of task and
675   category-related information during the Object Stimulus Period, with relative increases in the
676   size of task-related effects when moving up the visual cortical hierarchy.
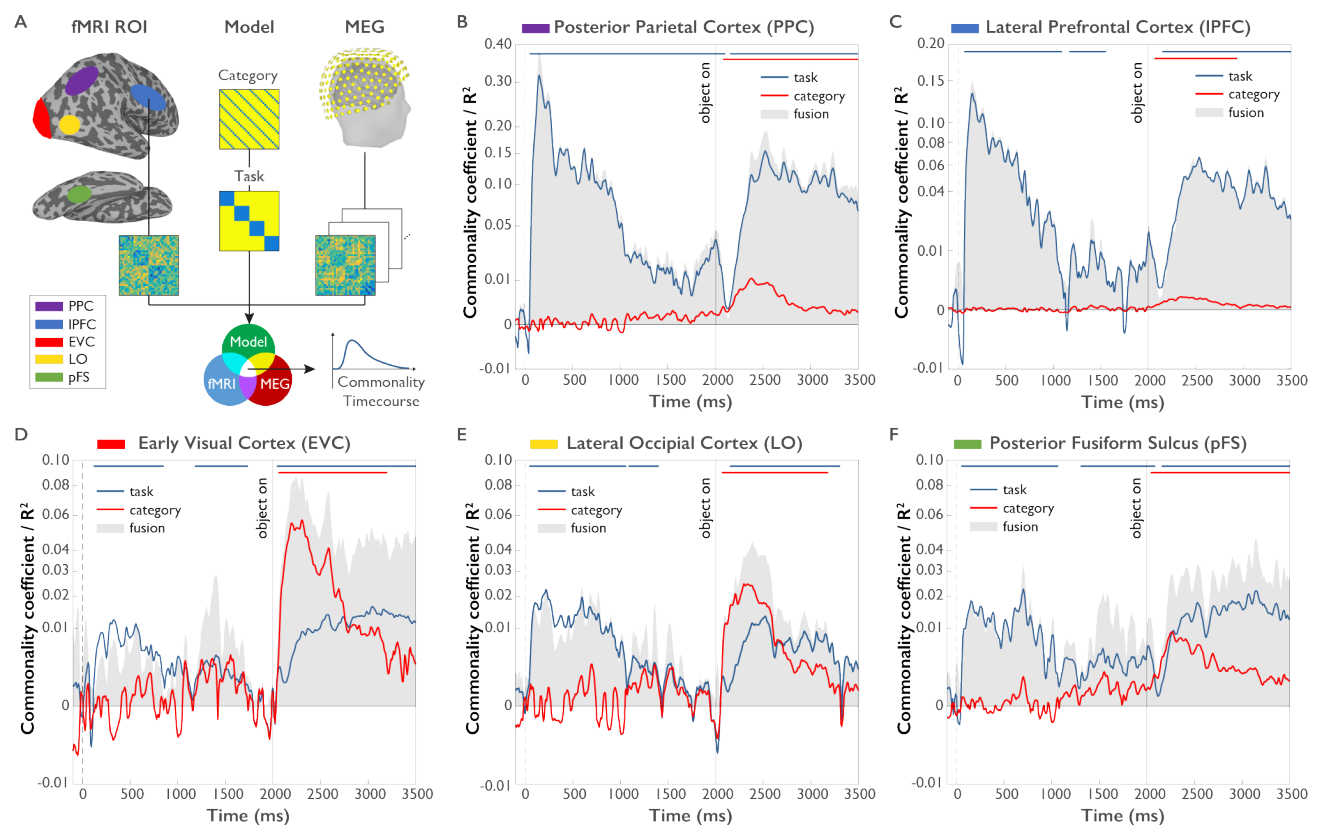
677

Figure 5. Model-based MEG-fMRI fusion procedure and results. **A.** Model-based MEG-fMRI fusion in the current formulation reflects the shared variance (commonality) between three dissimilarity matrices: (1) an fMRI RDM generated from voxel patterns of a given ROI, (2) a model RDM reflecting the expected dissimilarity structure for a variable of interest (e.g. task) excluding the influence of another variable of interest (e.g. category) and (3) an MEG RDM from MEG data at a given time point. This analysis was conducted for each MEG time point independently, yielding a time course of commonality coefficients for each ROI. **B-F.** Time courses of shared variance and commonality coefficients for five regions of interest (ROIs) derived from model-based MEG-fMRI fusion ($p < 0.05$, cluster-corrected randomization test, corrected for multiple comparisons across ROIs): PPC (Panel **B**), lPFC (Panel **C**), EVC (Panel **D**), LO (Panel **E**) and pFS (Panel **F**). Blue plots reflect the variance attributed uniquely to task, while red plots reflect the variance attributed uniquely to object category. Grey shaded areas reflect the total amount of variance shared between MEG and fMRI RDMs, which additionally represents the upper boundary of the variance that can be explained by task or category models.

16

692
693 **Discussion**
694
695 We used MEG and time-resolved multivariate decoding to unravel the representational dynamics
696 of task context, object category, and their interaction. Information about task was found rapidly
697 after onset of the task cue and throughout the experimental trial, which was paralleled by
698 information about object category after onset of the object stimulus. Temporal cross-decoding
699 revealed separate and overlapping task context-related processes, suggesting a cascade of
700 representations including visual and semantic encoding of the task cue, the retention of the task
701 rule, and its application to the object stimulus. Investigating the interaction of task context and
702 object category, we found evidence for late effects of task context on object category
703 representations, with differerences in the strength rather than the quality of category-related
704 MEG patterns. Finally, model-based MEG-fMRI fusion revealed that parietal and frontal regions
705 were dominated by effects of task, whereas occipitotemporal regions reflected a mixture of task
706 and object category representations following object presentation, with relative increases in task-
707 related effects over time and along the visual cortical hierarchy.
708
709 *Representational Dynamics of Task Context*
710
711 While previous fMRI studies investigated the cortical location of task effects on visual object
712 processing (Harel et al., 2014; Erez and Duncan, 2015; Bracci et al., 2017; Bugatus et al., 2017),
713 they could not provide insight into the temporal dynamics of task context. By manipulating task
714 context on a trial-by-trial basis we were able to (1) map out the temporal evolution of task
715 context effects across different stages of the trial, (2) uncover different stages of processing using
716 temporal generalization analysis, and (3) localize task context-related information to different
717 regions of the brain using model-based MEG-fMRI fusion.
718   The results from multivariate decoding and temporal generalization analyses indicate that
719 following initial encoding of visual and semantic information about task cue (Task Cue Period),
720 there was a weak but consistent short-term memory representation of this information, paralleled
721 by a representation of the task rule. Temporal generalization analysis additionally revealed that
722 after onset of the object stimulus (Object Stimulus Period) the task representation changed
723 abruptly. This result is in line with previous work in non-human primates (Sigala et al., 2008;
724 Stokes et al., 2013) demonstrating largely distinct representations of different task phases in
725 prefrontal cortex. Since the representation of task after object onset did not generalize to early
726 time periods during the initial processing of the task cue, this indicates that during object
727 category processing task context is likely not represented in a purely visual or semantic format.
728 Instead, our temporal generalization results suggest that at least part of the task-related
729 information after object onset reflects a representation of task rule that is applied to the visually-
730 presented object stimulus (Wallis et al., 2001; Stoet and Snyder, 2004; Bode and Haynes, 2009;
731 Woolgar et al., 2011). This interpretation is in line with a recent working memory study
732 reporting a reemergence of task rule-related MEG patterns during stimulus presentation (Peters
733 et al., 2016).
734   Of note, the representation of task context in monkey prefrontal cortex has been shown to
735 be even more dynamic than described above and not to generalize at all between different
736 periods of the task (Stokes et al., 2013). Since our results demonstrate phases of cross-
737 classification between these time periods, this suggests that in the present study the source of the

738 cross-classification between these periods of the task may not originate from prefrontal cortex,
739 but from other brain regions such as posterior parietal cortex. Indeed, this interpretation is
740 supported by our MEG-fMRI fusion results that show no significant prefrontal representations of
741 task context during the delay period prior to the onset of the object stimulus, but a representation
742 of task in posterior parietal cortex.
743
744 *Differential Involvement of Frontoparietal and Occipitotemporal Brain Areas in Task and*
745 *Object Category Representations*
746
747 Previous research has suggested a dominance of parietal and prefrontal cortex in representing
748 task context (Duncan, 2010; Woolgar et al., 2011), while the processing of object category has
749 been attributed to occipitotemporal cortex (Grill-Spector et al., 1999; Kravitz et al., 2010; Cichy
750 et al., 2011). More recently, this view has been challenged: First, object category representations
751 have been found – with some dependence on task context – in both parietal (Konen and Kastner,
752 2008; Jeong and Xu, 2016; Bracci et al., 2017) and prefrontal cortex (Harel et al., 2014; Erez and
753 Duncan, 2015; Bracci et al., 2017). Second, there is some evidence for task context effects in
754 occipitotemporal cortex, although the extent of such effects remains debated (Harel et al., 2014;
755 Erez and Duncan, 2015; Lowe et al., 2016; Bracci et al., 2017; Bugatus et al., 2017), and the time
756 course of any such effects has remained elusive.
757 Our model-based MEG-fMRI fusion results provide a nuanced spatiotemporal
758 characterization of task and object category representations in frontoparietal and
759 occipitotemporal cortex. Frontoparietal cortex was strongly dominated by task context, with
760 much weaker representations of object category. This result reinforces the notion that the
761 dominant role of frontoparietal cortex is the representation of task, with a secondary role in
762 representing object category. In contrast, in occipitotemporal cortex, responses reflected a
763 mixture of object category and task-related effects after object onset, with an increasing
764 dominance of task over time and along the visual cortical hierarchy from low- to high-level
765 visual cortex (EVC, LO, pFS). These results reveal that both task and object category are
766 encoded in parallel in the same regions of occipitotemporal cortex and suggests an increasing
767 role of task context in high-level visual cortex.
768 The finding of parallel effects of category and task suggests an interaction of task context
769 and object category already in occipitotemporal cortex. This result contrasts with the view of a
770 "passive" role of occipitotemporal cortex in the processing of object category, according to
771 which object representations are read out by prefrontal cortex (Freedman et al., 2003). Instead,
772 our results suggest that task biases late components of object processing along occipitotemporal
773 cortex, an influence that may originate in brain regions strongly dominated by task in
774 frontoparietal cortex (Waskom et al., 2014). In addition, our results suggest that this influence
775 may increase along the visual cortical hierarchy. Indeed, pFS but not EVC or LO was found to
776 represent task context immediately prior to object onset, suggesting that task context has the
777 potential to affect the early stages of visual processing through a top-down bias. This bias may
778 reflect a task-specific modulation of the representational strength of task-relevant object features
779 after object onset. The concurrent representation of both task and category in the same brain
780 region may be beneficial for optimizing the tuning of categorical brain responses to the demands
781 of the task.
782
783 *Interaction of Task Context and Object Category*

18

784
785   The direct investigation of the temporal dynamics of task context and object category
786   interactions revealed three key findings. First, we found that differences in object category
787   processing between low-level perceptual and high-level conceptual tasks emerged late in time,
788   suggesting a late top-down modulation of object processing after initial object processing has
789   been completed, arguing against an early expectation-related modulation of feedforward
790   processing. This result is consistent with a previous EEG study using natural images in an animal
791   and vehicle detection task, finding an initial category-related signal followed by a late task-
792   related response signaling the presence of a target stimulus (VanRullen and Thorpe, 2001).
793   Similarly, a more recent MEG study (Ritchie et al., 2015) reported results for visual category
794   processing in two different tasks (object categorization vs. letter discrimination) that are
795   indicative of late differences in task-dependent stimulus processing. Overall, these combined
796   results suggest that task representations affect late, rather than early processing of visual
797   information.
798   Second, object category-related information leveled off more slowly for conceptual than
799   perceptual tasks, indicating different neural dynamics for different task types. This suggests that
800   for conceptual tasks encoding and maintenance of object category may be beneficial for carrying
801   out the task, in contrast to perceptual tasks that do not necessitate categorical representations.
802   While differences in the difficulty of the tasks could account for this pattern of results, we found
803   no differences in response times or accuracy for the different tasks, arguing against the relevance
804   of task difficulty. In support of this view, a previous study emploing a speeded version of the
805   same tasks and categories found no differences in response times between tasks (Harel et al.,
806   2014).
807   Finally, while task context affected the separability of object-related MEG patterns
808   between task types, object classification showed no reduction in classification accuracy between
809   task contexts, indicating that the overall structure of those patterns did not change. This result
810   contrasts with our prior study demonstrating qualitatively different object-related patterns in
811   lateral prefrontal and high-level object-selective cortex (Harel et al., 2014). However, the
812   contribution of multiple brain regions to the MEG response may be masking an interaction
813   between object category and task context. Indeed, our MEG-fMRI fusion data suggest that both
814   task context and object category are being processed in parallel in pFS, although future work
815   with independent data will be needed to resolve this issue.
816
817   *Conclusions*
818
819   Our results suggest that task is represented in multiple distinct yet overlapping processing stages
820   and that the impact of task context during object processing occurs late in time. Our MEG-fMRI
821   fusion results support the view of strong task-related responses in frontoparietal regions, while
822   demonstrating the concurrent processing of both task and object category in occipitotemporal
823   regions. Our findings provide a nuanced spatiotemporally-resolved view of task processing
824   throughout the human cerebral cortex.
825
826
827   **References**
828

19

829   Bode S, Haynes J-D (2009) Decoding sequential stages of task preparation in the human brain.
830   Neuroimage 45:606-613.
831   Bracci S, Daniels N, de Beeck HO (2017) Task context overrules object- and category-related
832   representational content in the human parietal cortex. Cerebral Cortex:1-12.
833   Bugatus L, Weiner KS, Grill-Spector K (2017) Task alters category representations in prefrontal
834   but not high-level visual cortex. NeuroImage.
835   Carlson T, Tovar DA, Alink A, Kriegeskorte N (2013) Representational dynamics of object
836   vision: The first 1000 ms. Journal of Vision 13:1-19.
837   Chang C-C, Lin C-J (2011) LIBSVM: a library for support vector machines. ACM Transactions
838   on Intelligent Systems and Technology (TIST) 2:27.
839   Cichy RM, Chen Y, Haynes J-D (2011) Encoding the identity and location of objects in human
840   LOC. Neuroimage 54:2297-2307.
841   Cichy RM, Pantazis D, Oliva A (2014) Resolving human object recognition in space and time.
842   Nature Neuroscience 17:455-462.
843   Cichy RM, Pantazis D, Oliva A (2016) Similarity-based fusion of MEG and fMRI reveals spatio-
844   temporal dynamics in human cortex during visual object recognition. Cerebral
845   Cortex:bhw135.
846   Clarke A, Devereux BJ, Randall B, Tyler LK (2015) Predicting the time course of individual
847   objects with MEG. Cerebral Cortex 25:3602-3612.
848   DiCarlo JJ, Zoccolan D, Rust NC (2012) How does the brain solve visual object recognition?
849   Neuron 73:415-434.
850   Duncan J (2010) The multiple-demand (MD) system of the primate brain: mental programs for
851   intelligent behaviour. Trends in Cognitive Sciences 14:172-179.
852   Emadi N, Esteky H (2014) Behavioral demand modulates object category representation in the
853   inferior temporal cortex. Journal of Neurophysiology 112:2628-2637.
854   Erez Y, Duncan J (2015) Discrimination of visual categories based on behavioral relevance in
855   widespread regions of frontoparietal cortex. Journal of Neuroscience 35:12383-12393.
856   Freedman DJ, Riesenhuber M, Poggio T, Miller EK (2003) A comparison of primate prefrontal
857   and inferior temporal cortices during visual categorization. Journal of Neuroscience
858   23:5235-5246.
859   Greene MR, Baldassano C, Esteva A, Beck DM, Fei-Fei L (2016) Visual scenes are categorized
860   by function. Journal of Experimental Psychology: General 145:82-94.
861   Grill-Spector K, Kushnir T, Edelman S, Avidan G, Itzchak Y, Malach R (1999) Differential
862   processing of objects under various viewing conditions in the human lateral occipital
863   complex. Neuron 24:187-203.
864   Grootswagers T, Wardle SG, Carlson TA (2016) Decoding dynamic brain patterns from evoked
865   responses: A tutorial on multivariate pattern analysis applied to time series neuroimaging
866   data. Journal of Cognitive Neuroscience.
867   Harel A, Kravitz DJ, Baker CI (2014) Task context impacts visual object processing
868   differentially across the cortex. Proceedings of the National Academy of Sciences
869   111:E962-E971.
870   Hebart MN, Donner TH, Haynes J-D (2012) Human visual and parietal cortex encode visual
871   choices independent of motor plans. Neuroimage 63:1393-1403.
872   Hebart MN, Görgen K, Haynes J-D (2015) The Decoding Toolbox (TDT): a versatile software
873   package for multivariate analyses of functional imaging data. Frontiers in
874   Neuroinformatics 8:88.

875 Isik L, Meyers EM, Leibo JZ, Poggio T (2014) The dynamics of invariant object recognition in
876   the human visual system. Journal of Neurophysiology 111:91-102.
877 Jeong SK, Xu Y (2016) Behaviorally relevant abstract object identity representation in the
878   human parietal cortex. Journal of Neuroscience 36:1607-1619.
879 Kaiser D, Azzalini DC, Peelen MV (2016) Shape-independent object category responses
880   revealed by MEG and fMRI decoding. Journal of Neurophysiology 115:2246-2250.
881 King J, Dehaene S (2014) Characterizing the dynamics of mental representations: the temporal
882   generalization method. Trends in Cognitive Sciences 18:203-210.
883 Kok P, Jehee JF, de Lange FP (2012) Less is more: expectation sharpens representations in the
884   primary visual cortex. Neuron 75:265-270.
885 Kok P, Brouwer GJ, van Gerven MA, de Lange FP (2013) Prior expectations bias sensory
886   representations in visual cortex. Journal of Neuroscience 33:16275-16284.
887 Konen CS, Kastner S (2008) Two hierarchically organized neural systems for object information
888   in human visual cortex. Nature Neuroscience 11:224-231.
889 Kravitz DJ, Kriegeskorte N, Baker CI (2010) High-level visual object representations are
890   constrained by position. Cerebral Cortex 20:2916-2925.
891 Kriegeskorte N, Mur M, Bandettini PA (2008) Representational similarity analysis-connecting
892   the branches of systems neuroscience. Frontiers in Systems Neuroscience 2:4.
893 Lowe MX, Gallivan JP, Ferber S, Cant JS (2016) Feature diagnosticity and task context shape
894   activity in human scene-selective cortex. NeuroImage 125:681-692.
895 McKee JL, Riesenhuber M, Miller EK, Freedman DJ (2014) Task dependence of visual and
896   category representations in prefrontal and inferior temporal cortices. Journal of
897   Neuroscience 34:16065-16075.
898 Meyers EM, Freedman DJ, Kreiman G, Miller EK, Poggio T (2008) Dynamic population coding
899   of category information in inferior temporal and prefrontal cortex. Journal of
900   Neurophysiology 100:1407-1419.
901 Nichols TE, Holmes AP (2002) Nonparametric permutation tests for functional neuroimaging: a
902   primer with examples. Human Brain Mapping 15:1-25.
903 Pedhazur EJ (1997) Multiple Regression in Behavioral Research: Explanation and Prediction, 3
904   Edition. Orlando, FL: Harcourt Brace.
905 Peters B, Bledowski C, Rieder M, Kaiser J (2016) Recurrence of task set-related MEG signal
906   patterns during auditory working memory. Brain research 1640:232-242.
907 Riesenhuber M, Poggio T (2002) Neural mechanisms of object recognition. Current Opinion in
908   Neurobiology 12:162-168.
909 Ritchie JB, Tovar DA, Carlson TA (2015) Emerging object representations in the visual system
910   predict reaction times for categorization. PLoS Comput Biol 11:e1004316.
911 Seibold DR, McPhee RD (1979) Commonality analysis: A method for decomposing explained
912   variance in multiple regression analyses. Human Communication Research 5:355-365.
913 Serre T, Oliva A, Poggio T (2007) A feedforward architecture accounts for rapid categorization.
914   Proceedings of the National Academy of Sciences 104:6424-6429.
915 Sigala N, Kusunoki M, Nimmo-Smith I, Gaffan D, Duncan J (2008) Hierarchical coding for
916   sequential task events in the monkey prefrontal cortex. Proceedings of the National
917   Academy of Sciences 105:11969-11974.
918 Stoet G, Snyder LH (2004) Single neurons in posterior parietal cortex of monkeys encode
919   cognitive set. Neuron 42:1003-1012.

920 Stokes MG, Kusunoki M, Sigala N, Nili H, Gaffan D, Duncan J (2013) Dynamic coding for
921   cognitive control in prefrontal cortex. Neuron 78:364-375.
922 Tadel F, Baillet S, Mosher JC, Pantazis D, Leahy RM (2011) Brainstorm: a user-friendly
923   application for MEG/EEG analysis. Computational intelligence and neuroscience 2011:8.
924 Van de Nieuwenhuijzen M, Backus A, Bahramisharif A, Doeller C, Jensen O, van Gerven MA
925   (2013) MEG-based decoding of the spatiotemporal dynamics of visual category
926   perception. Neuroimage 83:1063-1073.
927 VanRullen R, Thorpe SJ (2001) The time course of visual processing: From early perception to
928   decision-making. Journal of Cognitive Neuroscience 13:454-461.
929 Wallis JD, Anderson KC, Miller EK (2001) Single neurons in prefrontal cortex encode abstract
930   rules. Nature 411:953-956.
931 Waskom ML, Kumaran D, Gordon AM, Rissman J, Wagner AD (2014) Frontoparietal
932   representations of task context support the flexible control of goal-directed cognition.
933   Journal of Neuroscience 34:10743-10755.
934 Woolgar A, Thompson R, Bor D, Duncan J (2011) Multi-voxel coding of stimuli, rules, and
935   responses in human frontoparietal cortex. Neuroimage 56:744-752.
936